Effects of structural defects and acid–basic properties on the activity and selectivity of isopropanol decomposition on nanocrystallite sol–gel alumina catalyst

J.A. Wang [a], X. Bokhimi [a], O. Novaro [a,*], T. López [b], F. Tzompantzi [b], R. Gómez [b], J. Navarrete [c], M.E. Llanos [c], E. López-Salinas [c]

[a] *Instituto de Fisica, Universidad Nacional Autónoma de México, A.P. 20-364, 01000 México D.F. Mexico*
[b] *Departmento de Quimica, Universidad Autónoma Metropolitana-I, A.P. 55-534, 09340 México D.F. Mexico*
[c] *Instituto Mexicano del Petroleo, Eje Central Lazaro Cardenas 125, 07730 México D.F. Mexico*

Abstract

The surface acid–basic properties of sol–gel alumina catalysts were studied by Fourier transform infrared (FTIR) spectroscopy of pyridine adsorption and temperature-programmed desorption of CO_2 and NH_3. The number of acid and basic sites on the samples varied with the calcination temperatures of the samples. The populations of the three different aluminum ions—tetrahedral, pentacoordinated and octahedral, which were identified by the ^{27}Al MAS NMR, were strongly affected by the sample calcination temperature and the crystalline composition. In the reaction temperature range between 100 and 250°C, isopropanol decomposition on sol–gel alumina catalysts was carried out. It was found that isopropanol decomposition on alumina catalyst was a structural-defect sensitive reaction. The dehydrogenation selectivity to acetone depended on the surface basic sites and the concentration of aluminum vacancies in the crystalline structure of γ-Al_2O_3. Bimolecular reaction to isopropylether was largely governed by the pentacoordinated aluminum ions which were related to the coordinately unsaturated aluminum ions. A mechanism for the formation of isopropylether was proposed: oxygen vacancies were suggested to involve the adsorption step of isopropanol, an intermediate species, $(CH_3)_2HC^+$, reacted with $(CH_3)_2HCO^-$ yielding isopropylether molecule. © 1999 Elsevier Science B.V. All rights reserved.

Keywords: Alumina; Catalyst; Sol–gel; Acid–basic site; Aluminum coordination; Structural defects; Isopropanol decomposition

1. Introduction

Alumina can be used not only as ceramics materials, but also as a carrier for catalysts and active component in acid–basic catalytic and petroleum refining reactions [1–6]. It is gener- ally obtained by calcining aluminum hydrox- ides. Its surface properties largely depend on its crystallographic structure and microporous tex- ture. In alumina phases, aluminum ions gener- ally occupy both tetrahedral and octahedral sites (Al^{IV} and Al^{VI}) [7–10]; however, in some cases, pentacoordinated aluminum ions (Al^V) can be also found [11,12]. Based on the observations of ^{27}Al NMR and EPR, Chen et al. [13] reported

* Corresponding author. Tel.: +52-5-616-1535; fax: +52-5-616-5032; e-mail: novaro@fenix.ifisicacu.unam.mx

that pentacoordinated aluminum ions are associated to Lewis acid sites. Hence, the effect of different aluminum coordinated environments on the surface acid–basic properties and therefore on the catalytic activity is a very interesting subject.

The surface acid–basic properties proved to play an important role in the acid–basic catalyzed reactions and can be characterized by a large number of techniques, for example, temperature-programmed desorption (TPD) of CO_2 and NH_3 and analyzed with Fourier transform infrared spectroscopy of pyridine adsorption [14,15]. On the other hand, the use of 2-propanol decomposition and other alcohols as a probe of the acid–basic sites is largely reported [16–26]. As a main assumption, the dehydrogenation of 2-propanol occurs on the surface basic sites and the dehydration is dependent of the acid sites on the surface of the catalyst.

Recent reports, however, show that dehydrogenation and dehydration of 2-propanol are not only determined by the acid or basic properties. These reactions are strongly affected by the experimental conditions, for example, reaction temperature, alcohol partial pressure and other factors. Rekoske and Barteau [27] report that when 2-propanol is decomposed on TiO_2 catalyst, selectivity to acetone significantly depends on the oxygen and water concentrations in the fed stream. The rate of 2-propanol dehydrogenation increases in the case of water presence, no matter whether it was produced by 2-propanol dehydration or added independently. In our recent work, using sol–gel MgO as catalyst, it was found that if we use the concept of 'basicity' proposed by Ai [28], to relate the experimental result, some adjustments such as the particle size effect must be taken into account [29].

In the present paper, we prepared sol–gel aluminum oxide catalyst from a homogenous medium and characterized it with different techniques. BET, ^{27}Al MAS NMR, FTIR-pyridine adsorption, NH_3-TPD and CO_2-TPD were used to investigate the specific surface area, pore size

distribution, aluminum coordination environment and the surface acid–basic properties of the catalyst, respectively. Isopropanol decomposition was used as the reaction probe to find the relationship between the acid–basic properties and dehydration or dehydrogenation selectivity in a wide reaction temperature range. The main aim of the present work is to analyze the influence of microstructure, aluminum coordination environment and surface acid–basic sites properties of sol–gel alumina catalyst on the activity and selectivity in the isopropanol decomposition.

2. Experimental

2.1. Preparation of the catalyst sample

The sol–gel catalysts were prepared by dissolving 25.73 ml aluminum trisecbutoxide (Aldrich, 99%) into a given amount of butanol; 1 g of oxalic acid (Baker, 99%), the hydrolysis catalyst, was added to this solution until having pH 5. Then 15 ml of water was slowly dropped into the solution. Afterwards, this solution was refluxed for 3 h at 70°C with continuous stirring until a gel was formed. The gel was dried at 70°C and calcined at 200, 400, 600 and 800°C.

2.2. Characterization

2.2.1. Specific surface area and pore size distribution analysis

Specific surface area and pore size distribution were obtained from nitrogen adsorption isotherms measured with an automatic ASAP 2000 analyzer.

2.2.2. ^{27}Al MAS NMR analyses

^{27}Al MAS NMR spectra were recorded using an ASX300 Bruker Instrument. The spectral frequency and width are 300.13 MHz and 50 000 Hz. All measurements were carried out at room temperature with a 10 μs pulse length (90°).

Table 1
Specific surface area, pore size distribution and pore volume of sol–gel alumina calcined at different temperatures

Temperature (°C)	BET surface area (m^2/g)	Micropore area (m^2/g)	Pore diameter (Å)	Total pore volume (cm^3/g)	Micropore volume (cm^3/g)
400	504.74	56.85	132.69	1.6744	0.02197
600	346.83	25.08	140.20	1.2157	0.00808
800	172.91		80.88	0.3497	

$Al(H_2O)_6^{3+}$ was used as the reference to measure the chemical shifts.

2.2.3. Temperature-programmed desorption of ammonia and carbon dioxide

The total basic and acidic sites of the catalyst were measured by TPD of CO_2 and NH_3 on an Altamira automatized apparatus. Before adsorption, the sample was heated in a He stream at 500°C for 30 min to desorb the impurities. Then, it was saturated with ammonia (carbon dioxide) for 30 min at 50°C. After the reactant excess was eliminated by flowing dry He at the same temperature, the sample was heated in steps of 10°C/min. The desorption signals were recorded by a computer through a thermal conductivity detector.

2.2.4. Pyridine adsorption Fourier transform infrared (FTIR)

Samples were characterized with a 170-SX FTIR spectrometer. Before pyridine adsorption, the sample in a vacuum was heated to 500°C at a rate of 20°C/min and then cooled to room temperature. It was then exposed for 20 min to pyridine (a capillary tube containing about 100

μl of pyridine in the spectrometer cell) by breaking. After adsorption for 30 min, its infrared spectrum was recorded at the temperature of interest with outgassing treatment.

2.3. Catalytic activity

The catalytic activity tests were performed on a flow microreactor–gas chromatography (MR–GC) system. Isopropanol was put in a double H-type saturator which was placed in a container. An ice–water mixture was held in this container for controlling the temperature of the saturator at 14°C. Nitrogen was used as carrier in all the tests. The partial pressure of isopropanol can be controlled with the temperature of the ice–water mixture. In this test, the partial pressure of isopropanol is 22.4 Torr. A total of 50 mg of catalyst sample was used in the activity measurements. The inlet rate is 10 ml/20 s. After the reaction was carried out for 15 min, the experimental data were recorded. In terms of the product distribution and total conversions, the selectivity for different products was calculated. All the data used to calculate the conversion and selectivity were averaged on

Table 2
Data of ^{27}Al MAS NMR of alumina samples calcined at different temperatures

Temperature (°C)	Population (%)			Position (ppm)		
	Tetrahedral	Pentacoordinated	Octahedral	P_t	P_p	P_o
400	13.0	16.5	70.5	61.53	33.06	5.58
600	17.3	18.7	64.0	65.32	35.30	5.42
800	22.6	12.2	65.2	63.59	35.76	4.91

P_t: position of tetrahedral coordination.
P_p: position of pentacoordination.
P_o: position of octahedral coordination.

three measurements done under the same conditions. When the reaction temperature was above 200°C, on the sample calcined at 400°C, a small amount of unidentified compounds in the products were found, but the total amount was lower than 1%. In the calculation of selectivity, overlooking these compounds would not give rise in a significant effect on the results; therefore, in the analysis presented in this article, we neglected these unknown compounds in our experimental results.

3. Results

3.1. Specific surface area, pore volume and pore size distribution

Data of the specific surface areas, pore size distribution and pore volume are shown in Table 1. The sample calcined at 400°C shows a large specific surface area (504.74 m^2/g) and a pore size of 132.69 Å. Increasing the calcination temperature from 400°C to 600 and 800°C results in BET surface areas decreasing from 504.74 m^2/g to 346.83 and 172.91 m^2/g, respectively. In the three samples, the microporosity increased when the calcination temperature

Fig. 2. In situ FTIR spectra of pyridine desorbed on the sample calcined at 600°C were recorded at different temperatures with evacuation.

is raised. These results indicate that thermal treatment process strongly affects the microstructure of the alumina samples.

3.2. Aluminum coordinated environment

Table 2 summarizes the estimated data of ^{27}Al MAS NMR. At 400°C, three peaks centered at 5.57, 33.06 and 61.53 ppm, were observed, indicating that aluminum atoms were surrounded by different neighbors. The peak at
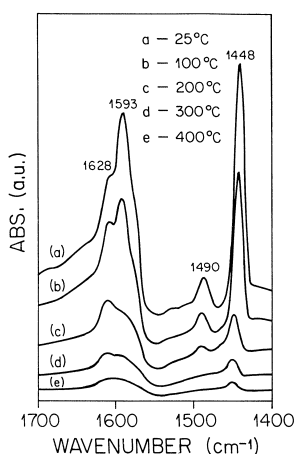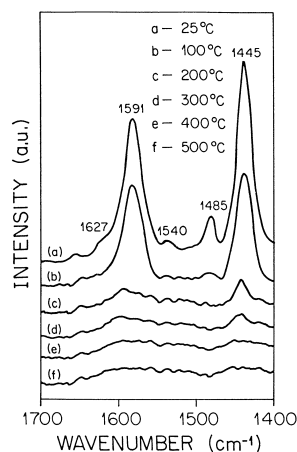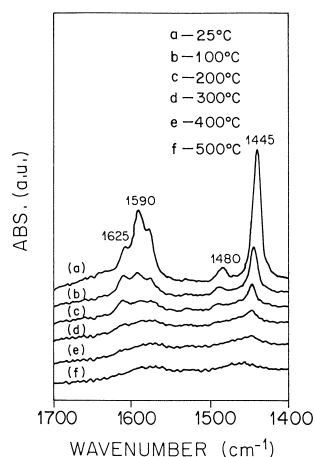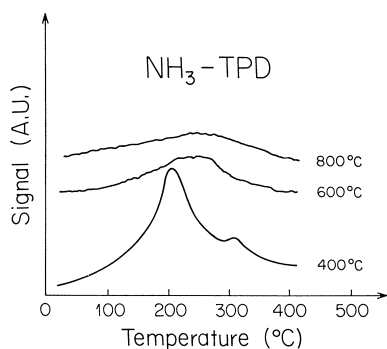

Fig. 1. In situ FTIR spectra of pyridine desorbed on the sample calcined at 400°C were recorded at different temperatures with evacuation.

Fig. 3. In situ FTIR spectra of pyridine desorbed on the sample calcined at 800°C were recorded at different temperatures with evacuation.

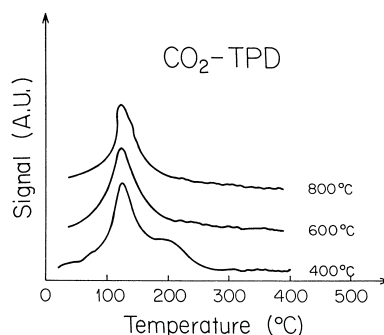Fig. 4. NH$_3$-TPD curves of the samples calcined at 400, 600 and 800°C.

Fig. 5. CO$_2$-TPD curves of the samples calcined at 400, 600 and 800°C.

5.57 ppm was a characteristic of octahedral aluminum ions, and the one located at 61.53 ppm was assigned to tetrahedral aluminum ions; while, the peak at 33.06 ppm, according to the reported data, can be ascribed to pentacoordinated aluminum ions [30–32]. Similarly, at 600 °C, three peaks appeared at 5.42, 35.30 and 65.32 ppm. However, when the sample was calcined at 800°C, the intensity of the signal at about 33 ppm decreased comparing to that observed in the sample calcined at 600°C. This was probably caused by ion rearrangement and the generation of structural defects during the phase transformation.

3.3. Surface acidity and basicity

FTIR-pyridine adsorption technique was used to determine the types of acid sites and NH$_3$-TPD was used to determine the total amount of acid sites.

Generally, in the infrared spectrum of pyridine adsorption on solids, the absorption bands at about 1577, 1490 and 1450 cm^{-1} are assigned to the different vibration modes of pyridine adsorbed on Lewis acid sites. The absorption band at 1540 cm^{-1} is believed as the characterization of pyridine adsorbed on Brønsted acid sites [33].

In the sample preheated at 400°C, three pyridine absorption bands, at 1448, 1490 and 1593 cm^{-1}, were observed (Fig. 1). This result showed that Lewis acidic sites were present. The intensities of all the bands gradually decreased when the desorption temperature increased; at 400°C of desorption, the three bands corresponding to Lewis sites nearly vanished. The band at 1628 cm^{-1} is ascribed to the vibration of hydroxyl ions bonded on the structures of the sample, which also diminishes due to its dehydroxylation when the temperature increased [34,35].

Table 3
Acid site concentration on the sol–gel alumina catalysts calcined at different temperatures

Temperature (°C)	T_{max1} (°C)	T_{max2} (°C)	M (μmol/g)
400	197	314	1410
600	275		422
800	267		142

T_{max1}: the central temperature of NH$_3$-TPD peak 1.
T_{max2}: the central temperature of NH$_3$-TPD peak 2.
M: the amount of NH$_3$ desorbed per gram of catalyst.

Table 4
Basic site concentration on the sol–gel alumina catalysts calcined at different temperatures

Temperature (°C)	T_{max1} (°C)	T_{max2} (°C)	M (μmol/g)
400	120	222	1270.7
600	102		1115.2
800	100		770.5

T_{max1}: the central temperature of CO$_2$-TPD peak 1.
T_{max2}: the central temperature of CO$_2$-TPD peak 2.
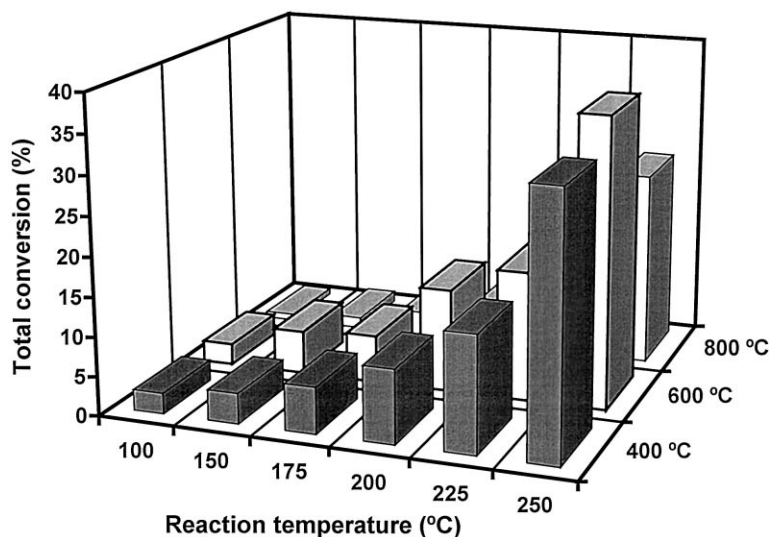M: amount of desorbed CO$_2$ per gram of catalyst.

Fig. 6. Total conversion of isopropanol decomposition on the samples calcined at 400, 600 and 800°C. Reaction was carried out in the temperature range between 100 and 250°C.

The pyridine adsorption spectra on the sample preheated at 600°C are shown in Fig. 2. Three absorption bands at 1445, 1485 and 1590 cm^{-1} were visible, indicating that Lewis acid sites were present on the surface of the sample. Increasing the desorption temperature from 25°C to 100, 200, 300 and 400°C, the relative inten-sity of the 1590 cm^{-1} band decreased from 8.69 to 5.00, 1.78, 0.70 and 0.23, respectively. Also, the relative intensity of the 1448 cm^{-1} band reduced from 0.89 to 0.08 when the desorption temperature increased from 25 to 400°C. At 500°C, both of the 1590 and 1448 cm^{-1} absorp-tion bands entirely disappeared. The band at
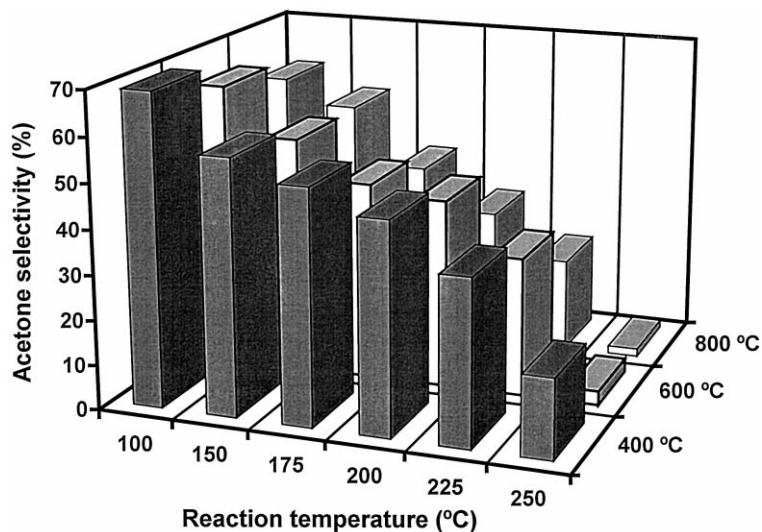

Fig. 7. Acetone selectivity as a function of the reaction temperature on the samples calcined at 400, 600 and 800°C. Reaction was carried out in the temperature range between 100 and 250°C.
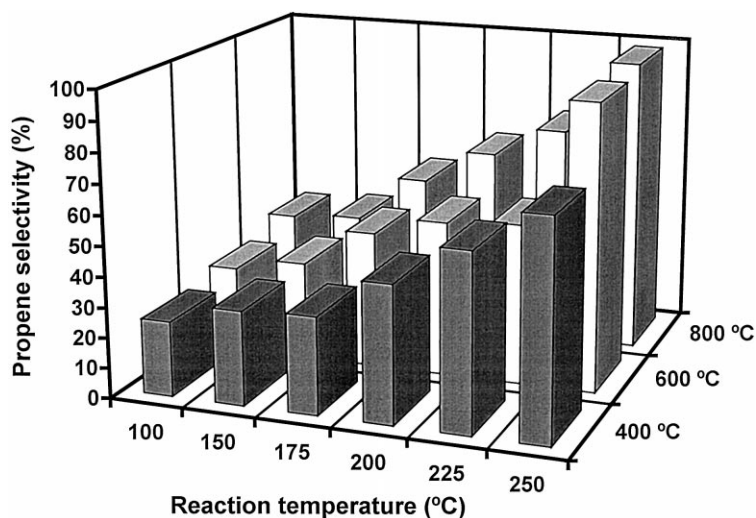
Fig. 8. Propene selectivity as a function of the reaction temperature on the samples calcined at 400, 600 and 800°C. Reaction was carried out in the temperature range between 100 and 250°C.

1627 cm^{-1} is also ascribed to the vibration of OH ion bonded on the samples.

The pyridine adsorption-FTIR spectra in the sample preheated at 800°C are shown in Fig. 3. The absorption bands assigned to Lewis acid sites were seen clearly, their temperature behavior was similar to that observed in the sample preheated at 600°C.

NH$_3$-TPD curves are shown in Fig. 4 and the data derived from them, in Table 3. For the sample preheated at 400°C, 1410 μmol NH$_3$/g were adsorbed. Two desorption peaks centered at 197°C and 305°C were found, which corresponded to two different types of acid sites. When the sample preheating temperature increased to 600 and 800°C, the amount of ad-
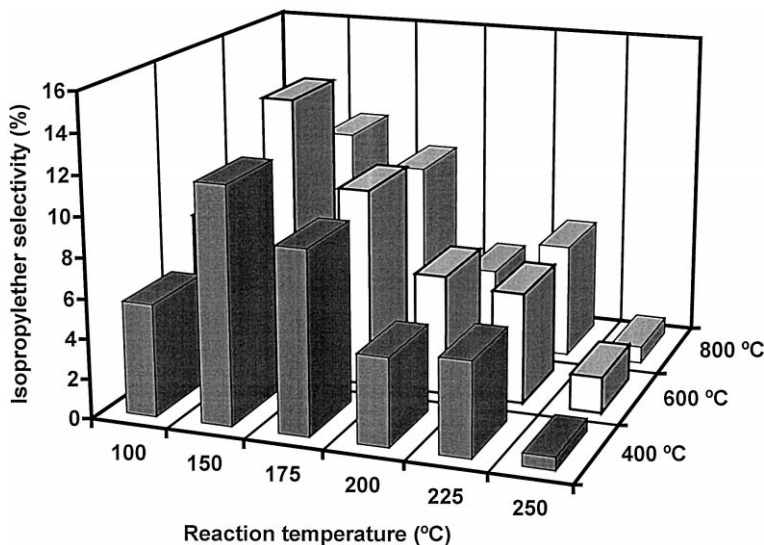

Fig. 9. Isopropylether selectivity as a function of the reaction temperature on the samples calcined at 400, 600 and 800°C. Reaction was carried out in the temperature range between 100 and 250°C.

Table 5
Conversion and selectivity of 2-propanol decomposition on sol–gel Al_2O_3 catalyst calcined at 400°C

Reaction temperature (°C)	Total conversion (%)	Selectivity (%)		
		Propene	Acetone	Isopropylether
250	33.04	71.64	27.71	0.65
225	14.76	58.41	36.85	4.74
200	9.38	45.31	47.07	4.42
175	5.91	37.18	52.22	9.17
150	3.88	31.19	56.96	11.86
100	2.66	24.81	69.55	5.64

sorbed ammonia significantly decreased to 422 and 142 μmol NH_3/g, respectively. Moreover, for these preheating temperatures, only one very weak adsorption peak centered at 275°C was observed.

The carbon dioxide TPD curves are shown in Fig. 5, and the data from them derived, in Table 4. When the sample calcined at 400°C, it had two CO_2 desorption peaks centered at 120 and 222°C, corresponding to the CO_2 adsorption amount of 1271 μmol/g. Of the three samples, this sample had the largest capacity of CO_2 adsorption. Samples preheated at 600 and 800°C, respectively, adsorbed 1115 and 771 μmol CO_2/g. Summarizing, the basicity decreased with the preheating temperature as the sequence: $B_{400} > B_{600} > B_{800}$.

3.4. Activity and selectivity of 2-propanol decomposition

The isopropanol decomposition reactions on Al_2O_3 catalysts were carried out at tempera-

tures ranging from 100 to 250°C. Isopropanol partial pressure was fixed at 22.4 Torr. Total conversions are shown in Fig. 6. The selectivity for dehydrogenation to acetone, dehydration to propylene and bimolecular reaction to isopropylether on the samples calcined at 400, 600 and 800°C, are shown in Figs. 7–9 and Tables 5–7.

The total conversion of isopropanol decomposition increased with the increasing reaction temperature. At different reaction temperatures, the sequence of the total conversion was $C_{600} > C_{400} > C_{800}$, showing that a high concentration of active sites were present in the sample calcined at 600°C. In comparison with the data shown in Figs. 7–9, we found that the selectivity of dehydrogenation to acetone decreased as the reaction temperature increased. On the contrary, the selectivity of dehydration to propene increased when the reaction temperature increased. The selectivity to isopropylether with the reaction temperature, however, varied: first, it increased with the reaction temperature ranging from 100 to 150°C, and then reached a

Table 6
Conversion and selectivity of 2-propanol decomposition on sol–gel Al_2O_3 catalyst calcined at 600°C

Reaction temperature (°C)	Total conversion (%)	Selectivity (%)		
		Propene	Acetone	Isopropylether
250	36.89	95.10	3.09	1.81
225	16.46	53.26	31.14	5.60
200	10.01	51.61	42.35	6.04
175	6.03	45.47	44.51	10.02
150	3.91	32.56	53.18	14.26
100	2.69	28.24	63.87	7.89

Table 7

Conversion and selectivity of 2-propanol decomposition on sol–gel Al_2O_3 catalyst calcined at 800°C

Reaction temperature (°C)	Total conversion (%)	Selectivity (%)		
		Propene	Acetone	Isopropylether
250	24.80	98.00	1.71	0.86
225	11.25	73.20	20.99	5.81
200	4.78	63.14	30.76	4.10
175	3.20	51.58	40.12	9.30
150	1.41	35.64	53.55	10.81
100	0.79	34.01	59.04	6.95

maximum value at 150°C; afterwards, it diminished when the reaction temperature increased. When we compare the different selectivity of isopropanol decomposition on these three samples, some differences were found. For example, on the sample calcined at 400°C, at the reaction temperature of 100°C, the selectivity of dehydrogenation to acetone was 69.55%; but on the samples calcined at 600°C and 800°C, the selectivity was 63.87 and 59.04%, respectively, showing an increasing sequence of $S_{800} < S_{600} < S_{400}$. At other reaction temperatures, the similar sequence was also found. However, for the selectivity to propene, an inverse sequence was found: $S_{800} > S_{600} > S_{400}$. All these results indicated that the activity and selectivity of the decomposition reaction of isopropanol depended on the calcination temperature of the catalysts and the reaction temperature.

4. Discussion

The calcination temperature markedly altered the population of aluminum ions in different coordination environments. For example, when the calcination temperature increased from 400 to 600°C, the population of the pentacoordinated aluminum ions increased; at 800°C, however, it diminished. In our previous work, studies of XRD and TG-DTG showed that when the sample was calcined at 400°C for 8 h, AlO(OH) (boehmite) and γ-Al_2O_3 phases coexisted [36]. There are 4 aluminum ions and 12 OH groups in the unit cell of AlO(OH). In the structure of

boehmite, its lattice cell consists of two closed-packing layers of OH groups separated by a layer of Al ions in octahedral positions. Since some oxygen vacancies produced during the dehydroxylation were found in octahedral positions in the AlO(OH) structure, therefore, the neighbors of some octahedral aluminum ions were unsaturated [36]. Because an aluminum ion in octahedral position surrounded by six oxygen neighbors, if one oxygen ion is absent, an oxygen defect site is hence created. In those oxygen vacancies, the electron density is larger than that produced by the tetrahedral oxygen, but smaller than that produced by the octahedral oxygen, a chemical shift can hence be yielded. Therefore, it is expected that a signal between the normal tetrahedral and octahedral aluminum ions can be observed in the ^{27}Al MAS NMR spectra. The population of pentacoordinated aluminum ions is related to the unsaturated aluminum coordination environments.

The number of unsaturated aluminum ions, however, is affected by the different phase composition of the samples. For example, at 600°C, the sample had γ-Al_2O_3 and θ-Al_2O_3. θ-Al_2O_3 had oxygen vacancies in its structure, which decreased when the sample calcination temperature increased from 600 to 800°C [36]. Hence, the population of petancoordinated aluminum atoms was altered not only with the calcination temperature but also with the phase composition.

The population of tetrahedral aluminum ions also varied with the calcination temperature. It increased when the calcination temperature in-
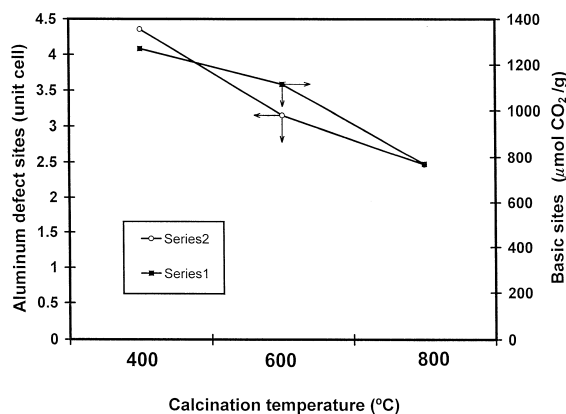
Fig. 10. Aluminum vacancies and basic sites as a function of calcination temperature. Series 1: Amount of adsorbed CO_2; Series 2: Aluminum vacancies/unit cell in the structure of γ-Al_2O_3.

creased. Because in the lattice cells of γ-Al_2O_3, aluminum ions occupy both octahedral and tetrahedral positions. However, aluminum ions in the unit cell of AlO(OH) only occupy octahedral positions. At 400°C, about 11.51% boehmite phase coexisted with γ-Al_2O_3; but at 600°C, boehmite phase disappeared. Hence, the phase transformation from AlO(OH) to γ-Al_2O_3 seems to be responsible for the difference of the population of tetrahedral aluminum ions between the samples calcined at 400 and 600°C. When the sample was calcined at 600 and 800°C, γ-Al_2O_3 and θ-Al_2O_3 phases were identified, however, the phase composition was different: about 7.81% increment in θ-Al_2O_3 phase at 800°C was found in comparison to that at 600°C. In the unit lattice cell of the normal θ-Al_2O_3 phase, about 75% Al ions occupy tetrahedral positions. This means that the ratio of Al^{IV} to Al^{VI} is about 3 in the normal θ-Al_2O_3 phase, which is higher than the one in the lattice cell of normal γ-Al_2O_3 phase, in which the ratio of Al^{IV} to Al^{VI} is about 2. On the other hand, the reduction of the population of pentacoordinated aluminum ions with the increasing of the calcination temperature also has an effect on the distribution of tetrahedral and octahedral aluminum ions. Thus, compared to that at 600°C, the slight increment of the tetrahedral aluminum popula-

tion at 800°C can be largely explained by the phase transformation.

Taking into account the acid–basic properties, as shown in Figs. 4 and 5, the sample calcined at 400°C adsorbed the largest amount of CO_2 and NH_3, hence, it had the biggest number of basic and acid sites. In addition, for both CO_2 and NH_3 desorption, two desorption peaks were found. These results show that there are two types of acid sites and two types of basic sites in this sample. Probably it was caused by the mixture of the phases, because 11.86% AlO(OH) phase coexisted with γ-Al_2O_3 in this sample.

Some aluminum vacancies existed in both tetrahedral and octahedral positions in the structure of γ-Al_2O_3 phase from the results of Rietveld refinements [36]. The total number of these vacancies decreased from 4.36 to 3.15 and 2.47/unit cell when the calcination temperature increased from 400°C to 600 and 800°C. Both the number of aluminum vacancies and the number of basic sites decreased as a function of calcination temperature, which suggests that the aluminum vacancies can yield the basic sites (Fig. 10).

The relationship between the selectivity of dehydrogenation to acetone and the number of
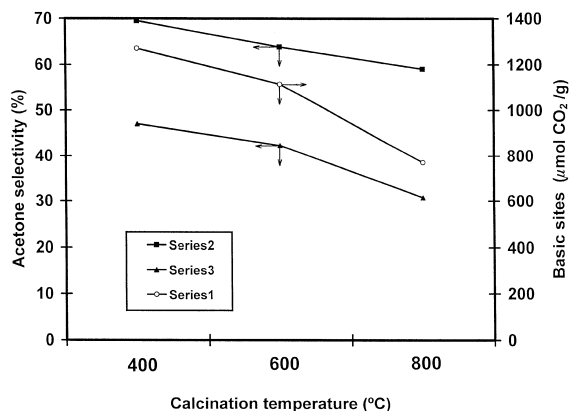

Fig. 11. Acetone selectivity and basic sites as a function of calcination temperature. Series 1: Amount of adsorbed CO_2; Series 2: Acetone selectivity at the reaction temperature of 100°C; Series 3: Acetone selectivity at the reaction temperature of 200°C.
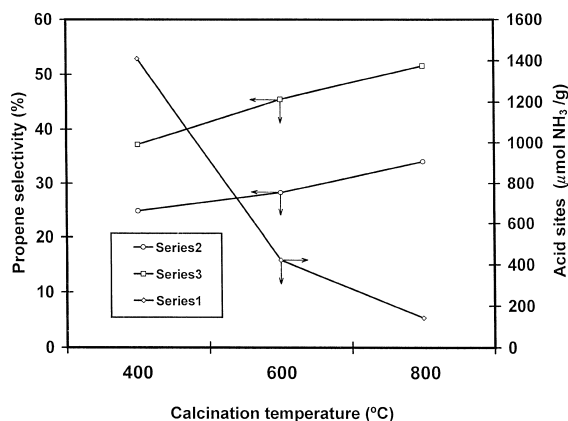
Fig. 12. Propene selectivity and acid sites as a function of calcination temperature. Series 1: Amount of NH_3 adsorbed on the samples; Series 2: Propene selectivity at the reaction temperature of 100°C; Series 3: Propene selectivity at the reaction temperature of 175°C.

basic sites is reported in Fig. 11. On one hand the selectivity of dehydrogenation to acetone for all three samples at different reaction temperatures decreased when the calcination temperature increased; on the other hand, the number of basic sites also diminished with the calcination temperature. These results indicate that the formation of acetone depends on the surface basicity. As discussed above, basic sites are determined by the Al vacancies in the structure. Therefore, the selectivity for dehydrogenation to acetone is also dependent of the aluminum va-

cancies. This is not surprising for us because vacancies in the structures of the catalysts are often regarded as the active centers in the surface reactions. On the basis of this result, we can draw a conclusion that the structural vacancies play an important role in the decomposition of isopropanol and are probably the main factor for acetone formation.

There is no correlation between the selectivity for propene and the number of the acid sites (Fig. 12). The propene selectivity increased with the calcination temperature. The total amount of adsorbed ammonia, however, decreased when the calcination temperature increased. Even when we added the effect of the surface area, their relationship could not be found yet since the number of acid sites/nm^2 still decreased from 1.7 to 0.7 and 0.2 when the calcination temperature increased from 400°C to 600 and 800°C. This result suggests that the dehydration selectivity to propene does not strictly depend on the surface acid sites, disagreeing with the results reported by Luy and Parera [17].

Several mechanisms for acetone formation were presented. One of those is that α-H absorption step is involved in the dehydrogenation reaction [27,37]. This postulate can be supported by the results of the present study. As discussed above, the aluminum vacancies were proposed
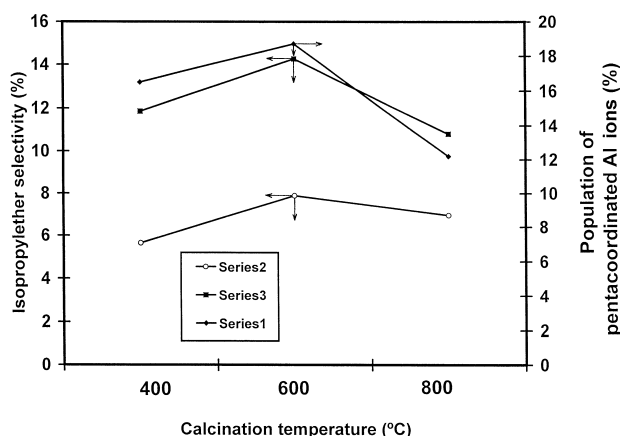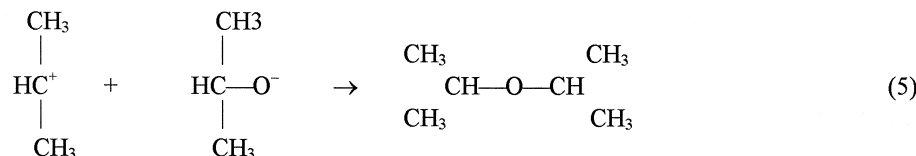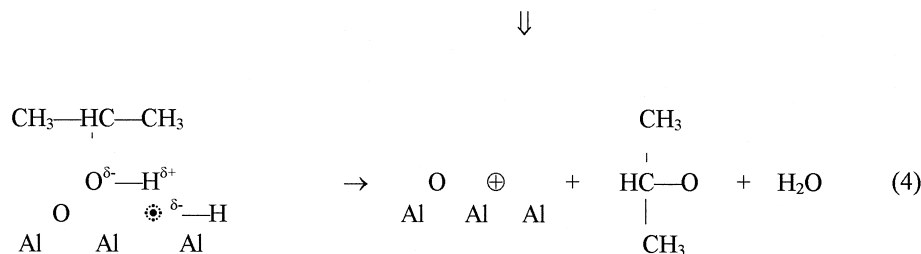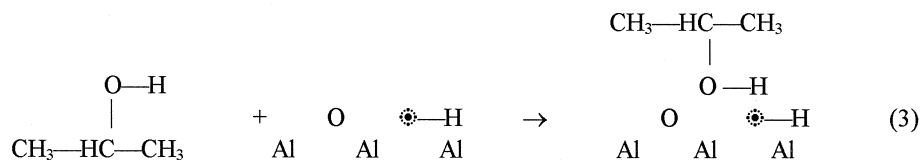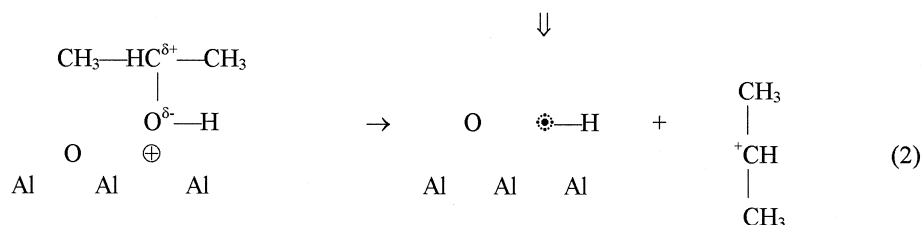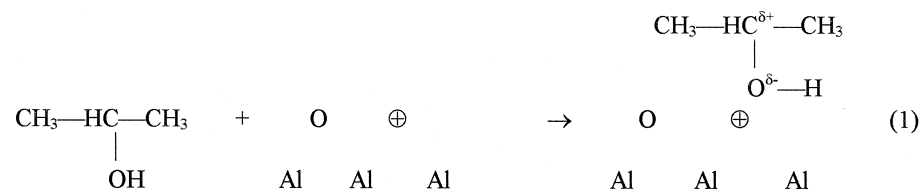

Fig. 13. Isopropylether selectivity and the population of pentacoordinated aluminum ions as a function of calcination temperature. Series 1: Population of pentacoordinated aluminum ions; Series 2: Isopropylether selectivity at the reaction temperature of 100°C; Series 3: Isopropylether selectivity at the reaction temperature of 150°C.

to involve in the formation of acetone. Because each aluminum vacancy is surrounded by oxygen ions and hence it has many negative charges; therefore, α-H can be easily adsorbed on these sites.

The behaviors of bimolecular reaction to form isopropylether are different for the three samples. For example, the selectivity to isopropylether was 5.64 and 11.86% on the sample calcined at 600°C at the reaction temperature of 100 and 150°C; however, for the samples calcined at 400 and 800°C, isopropylether selectivity was 7.89 and 6.95% at 100°C, 14.26 and 10.81 at 150°C, respectively. These results show that the selectivity to isopropylether on the sample calcined at 600°C is the highest. The isopropylether selectivity has the following sequence: $S_{600} > S_{400} > S_{800}$. This sequence is

Scheme 1. A mechanism of isopropylether formation on alumina catalyst (⬡ oxygen defect site; ⬡—H adsorbed OH group).

similar to the one of the number of pentacoordinated aluminum ions in the samples as a function of calcination temperature (Fig. 13).

As discussed above, the pentacoordinated aluminum ions correlated to the oxygen vacancies existing in the structures of both boehmite and θ-Al_2O_3 phases. Therefore, the generation of pentacoordinated aluminum ions seems to be relation to the boehmite and θ-Al_2O_3 phases. In these three samples, the concentration of both boehmite and θ-Al_2O_3 was lower than that of γ-Al_2O_3, the total number of the oxygen vacancies in these two phases was relative small. Therefore, there were not many active centers for the bimolecular reaction to form isopropylether, and the isopropylether concentration in the products was hence no more than 15%.

We assumed that the formation of isopropylether depends on the oxygen vacancies (coordinately unsaturated aluminum ions) and this suggested mechanism is shown in Scheme 1. In the first step, because many positive charges existed on the oxygen vacancies, an isopropanol molecule could adsorb on an oxygen defect site, an intermediate with positive charge, $(CH_3)_2HC^+$, and an adsorbed hydroxyl species bonded to the oxygen defect site were formed owing to the interaction and the transferring of the electrons between the adsorbed species and the defect site. In the next step, another isopropanol molecule attacked the adsorbed OH group, resulting in an intermediate with negative charge, $(CH_3)_2HCO^-$, and a water molecule being yielded. Finally the positive charge species reacting with the negative charged led to the generation of isopropylether.

The further work for detecting the intermediates to support the above suggested mechanism of isopropylether formation will be carried out.

5. Conclusions

Selectivity in the isopropanol decomposition on sol–gel alumina catalysts was shown to be a function not only of the surface acid–basic properties but also of the structural defects of the aluminum oxide. In contrast to the conventional concept, the selectivity of dehydration to propene did not strictly depend on the surface acidic site concentration. The selectivity of dehydrogenation to acetone, however, depended on the surface basic sites of the catalyst. We found that the selectivity of dehydrogenation can also be determined by the concentration of the cation defects in the lattice cell. The defects in the crystalline structure play an important role in the isopropanol decomposition, especially in the pathway of dehydrogenation, which is often overlooked in the surface acid–basic studies.

A mechanism of isopropylether formation was proposed based on the fact that the population of pentacoordinated aluminum ions as a function of calcination temperature is similar to the one of the selectivity for bimolecular reaction to isopropylether altering with the calcination temperature. In this mechanism, we suggested that oxygen defects involved in the adsorption step of isopropanol. A positively charged intermediate reacting with negatively charged species yields isopropylether and water.

References

[1] J.D. Mackenzie, D.R. Ulrich, Ultrastructure Processing of Ceramics, Glasses and Composites, Wiley, New York, 1988.
[2] B.E. Yoldas, J. Am. Chem. Soc. 65 (1982) 387.
[3] B.E. Yoldas, Transparent activated nanoparticle alumina and method of preparing sample, U.S. Patent, 3941719, 1976.
[4] T. López, R. Gómez, in: L.C. Klein (Ed.), Sol–gel Optics, Kluwer Academic, Boston, 1994, 345 pp.

[5] J.B. Peri, J. Phys. Chem. 69 (1965) 211.

[6] J. Koubec, J. Volf, J. Pesek, J. Catal. 38 (1975) 385.

[7] E. Lippen, A. Samoson, Magi, J. Am. Chem. Soc. 108 (1986) 6158.

[8] R.J. Pellet, C. Scott-Blackwell, J.A. Rabo, J. Catal. 114 (1988) 71.

[9] R.P. Man, J. Klinowsky, Chem. Phys. Lett. 147 (1988) 581.

[10] J. Sanz, V. Fornes, A. Corma, J. Chem. Soc. Faraday Trans. 84 (1988) 3113.

[11] C.W. Burnham, M.J. Buerger, Z. Kristallogr. 115 (1961) 269.

[12] Y. Oka, T. Takahashii, K. Okada, S. Iwai, J. Non-Cryst. Solids (1979) 349.

[13] F.R. Chen, J.G. Davis, J.J. Fripiat, J. Catal. 133 (1992) 263.

[14] P. Berteau, M. Kellens, B. Delmon, J. Chem. Soc. Faraday Trans. 87 (1991) 1452.

[15] T. López, J. Navarrete, R. Gómez, O. Novaro, F. Figueras, H. Armendariz, Appl. Catal. A: General 125 (1995) 217.

[16] A. Gervasini, A. Auroux, J. Catal. 131 (1991) 190.

[17] J.C. Luy, J.M. Parera, Appl. Catal. 26 (1986) 295.

[18] M.R. Mostafa, A.M. Youssef, S.M. Hassan, Mater. Lett. 12 (1991) 207.

[19] J. Cunningham, B.K. Hodnett, M. Iiyas, J. Tobin, E.L. Leahy, J.L. Fierro, Faraday Discussions 72 (1981) 283.

[20] M. Ai, Bull. Chem. Soc. Jpn. 50 (1977) 2579.

[21] M. Ai, Bull. Chem. Soc. Jpn. 49 (1976) 1328.

[22] M. Ai, Bull. Chem. Soc. Jpn. 47 (1974) 3074.

[23] M. Ai, S. Suzuki, Bull. Chem. Soc. Jpn. 46 (1973) 321.

[24] M. Ai, J. Catal. 40 (1975) 318.

[25] M. Ai, J. Catal, J. Catal. 50 (1977) 291.

[26] T. López, M. Asomoza, R. Gómez, J. Non-Cryst. Solids 147 (1992) 769.

[27] J.E. Rekoske, M.A. Barteau, J. Catal. 165 (1997) 57.

[28] M. Ai, Bull. Soc. Chem. Jpn. 50 (1977) 355.

[29] R. Portillo, T. López, R. Gómez, X. Bokhimi, A. Morales, O. Novaro, Langmuir 12 (1996) 40.

[30] F.R. Chen, J.G. Davis, J.J. Fripiat, J. Catal. 133 (1992) 263.

[31] R. Dupree, I. Farnan, A.J. Forty, S. El-Mashri, L. Bottyan, J. Phys. Colloq. 46 (1985) 113.

[32] G.A. Pozarnsky, A.V. McCormick, J. Non-Cryst. Solid 190 (1995) 212.

[33] J. Ward, Zeolite chemistry and catalysis, in: J.A. Rabo (Ed.), ACS Monograph 171, Am. Chem. Soc., Washington, DC, 1976.

[34] A. Vázquez, T. López, R. Gómez, X. Bokhimi, A. Morales, O. Novaro, J. Solid State Chem. 128 (1997) 161.

[35] T. López, R. Marmolejo, M. Asomoza, S. Solís, R. Gómez, J.A. Wang, X. Bokhimi, O. Novaro, J. Navarrete, M.E. Llanos, E. López, Mater. Lett. 32 (1997) 325.

[36] J.A. Wang, O. Novaro, X. Bokhimi, T. López, R. Gómez, J. Catal. (submitted).

[37] M. Bowker, R.W. Petts, H.D. Vandervell, J. O'Malley, Appl. Catal. 25 (1986) 121.